Theory for the Elementary Time Scale of Stress Relaxation in Polymer Nanocomposites

Yuxing Zhou and Kenneth S. Schweizer*

Cite This: *ACS Macro Lett.* 2022, 11, 199−204

Read Online

ACCESS | Metrics & More | Article Recommendations | Supporting Information

ABSTRACT: We construct a microscopic theory for the elementary time scale of stress relaxation in dense polymer nanocomposites. The key dynamical event is proposed to involve the rearrangement of cohesive segment-nanoparticle (NP) tight bridging complexes via an activated small NP dilational motion, which allows the confined segments to relax. The corresponding activation energy is determined by the NP bridge coordination number and potential of mean force barrier. The activation energy varies nonlinearly with interfacial cohesion strength and NP concentration, and a universal master curve is predicted. The theory is in very good agreement with experiments. The underlying ideas are relevant to a variety of other hybrid macromolecular materials involving hard particles and soft macromolecules.
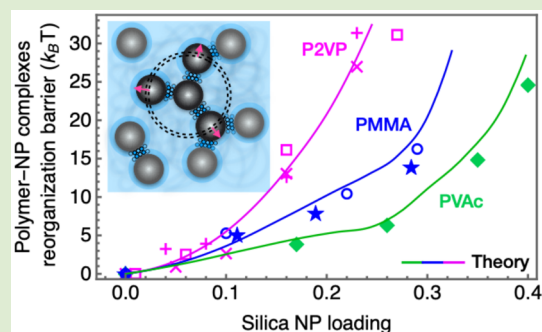
Polymer nanocomposites (PNCs) are fascinating hybrid soft matter systems typically composed of spherical rigid nanoparticles dissolved in dense random coil polymer matrices. They exhibit many appealing properties relevant to materials science, colloid science, and even biology.[1−4] PNC dynamics[5−7] is rich and challenging to understand due to the enormous amount of (often strongly cohesive) internal curved surface area, complex microstructure, presence of multiple length/time/energy scales, and large parameter space including composition, nanoparticle (NP) size, temperature, interfacial cohesion strength, and polymer degree of polymerization, *N*.

The dynamic complexity in PNCs is strikingly revealed in the linear viscoelastic response which probes collective stress relaxation associated with coupled NP and polymer motions over a wide range of time scales. A cluster sol−gel dynamic percolation model[8] captures reasonably well the isothermal frequency and NP loading dependences of the viscoelastic behavior based on two key assumptions:[8] (i) the large majority of the polymer matrix is essentially unperturbed by NPs and serves as a viscous background for cluster motion and (ii) rubbery polymer bridges connect NPs and act as effectively permanent bonds for NP cluster formation. Dielectric measurements[9−11] confirm assumption (i), from the segmental to macromolecular scale. Taken literally, assumption (ii) implies the anchoring segments of bridges do not desorb on the probed time scales, which is consistent with the observation of an ultralow frequency elastic modulus plateau[10] beyond the bond percolation threshold. However, bridging "bonds" are not literally static and undergo slow local dynamics on the experimental time scale.[9−14]

The fundamental question of the temperature dependence of the stress relaxation time underlies the ability to construct master curves of the viscoelastic storage and loss moduli as encoded in a rheological "shift factor" that sets the elementary time scale of slower and larger length scale dynamical processes (time−temperature superposition).[9,10,15] Its observed strong dependence on NP loading suggests the presence of a dissipative relaxation process associated with local rearrangement of polymer−NP complexes (pairs of NPs tightly bridged by polymer segments), in addition to the usual friction due to interpolymer forces. Recent experiments argued the elementary relaxation time for viscoelastic response is[10]

$$\tau_{\mathrm{rheo}}(T) \approx \tau_{\mathrm{poly}}(T)e^{\beta \Delta E} \qquad (1)$$

where β is the inverse thermal energy $(1/k_{\mathrm{B}}T)$, $\tau_{\mathrm{poly}}(T)$ is the structural or alpha time of the matrix polymers, and ΔE phenomenologically defines an activation energy for bridging complex relaxation based on viscoelastic data, the microscopic origin of which is not known. The ratio of $\tau_{\mathrm{rheo}}(T)$ at two different temperatures defines the viscoelastic shift factor. Analysis of experimental data[9,16] using eq 1 suggests that when polymer size $(2R_{\mathrm{g}})$ is comparable to or larger than the NP diameter $(D = 2R$; see Table S1$)$, ΔE is nearly N-independent. Systematic exploration of the dependence of ΔE on D is largely absent given the interest in nanoscale materials where typically

$D \sim 10-20$ nm. Strikingly, experiments find ΔE can be very large and varies strongly with both NP loading and interfacial attraction[9,10,16] (see Figure S1); for example, in silica-based PNCs, $\Delta E \sim 25 k_B T$ at room temperature for PVAc at 40% loading, and $\Delta E \sim 5$, ~ 10, and $\sim 30 k_B T$ at 20% loading as polymer chemistry changes from PVAc to PMMA to P2VP,[17] respectively, corresponding to increased interfacial attraction. These dependences of ΔE on adsorption energy (ϵ_{pn}) and NP concentration are not understood.

Our goal is to develop the first microscopic statistical mechanical theory for the fundamental energy scale ΔE. A recent speculative phenomenological model[10] postulated the equilibrium number of rubbery bridges per NP controls ΔE, apparently invoking bridge desorption as the origin of local dissipation. It assumes ΔE scales as the mean areal density of bridges which was crudely estimated based on de Gennes' analysis[18] of a chain confined between two parallel flat and nonadsorbing surfaces separated by $\langle h_{IPS} \rangle$. This analysis yields $\Delta E \sim \epsilon_{pn} \langle h_{IPS} \rangle^{-2}$, where $\langle h_{IPS} \rangle \approx 2R \left[(\phi_{RCP}/\phi)^{1/3} - 1 \right]$ is the mean interparticle surface-to-surface distance assuming a random microstructure, with ϕ the NP packing fraction and ϕ_{RCP} its random close packing value. The ϕ dependence of ΔE follows from $\langle h_{IPS} \rangle$ decreasing from $\sim R_g$ at low ϕ to the segment or Kuhn scale at high ϕ, independent of ϵ_{pn} by assumption.[10] Curiously, this postulate is qualitatively the same as invoked in the sol−gel cluster model[8] but for an entirely different property, the elementary elastic modulus, $G_{PN} \sim \langle h_{near} \rangle^{-2}$. Here, $\langle h_{near} \rangle$ is a mean nearest neighbor NP spacing defining the characteristic rubbery bridge size,[8] which was computed using an oversimplified hard-sphere fluid model. We are not advocating the $\Delta E \sim \langle h_{IPS} \rangle^{-2}$ ansatz as a causal explanation of the dynamical shift factor physics, but recent experiments find that it empirically captures quite well the ϕ dependence for some,[9,10] but not all,[16] PNCs, and worsens if $\langle h_{near} \rangle$ is used as the characteristic bridge size[8] (see Figure S2).

Why an entropic elastic shear modulus and segment-scale activation barrier should follow an identical dependence on NP loading is a conceptual puzzle. Moreover, the bridging chain desorption scenario for ΔE conflicts with the sol−gel cluster model based on very long-lived bonds,[8,19] the existence of a low frequency elastic plateau,[10] and the "glassy bridge" concept which does not address the shift factor problem.[20,21] It also conflicts with the fact that the NP microstructure is not random but exhibits strong polymer-mediated NP local clustering, per many theoretical,[22−24] simulation,[25−28] and (indirectly) scattering measurements.[29] The latter studies find the strongest bridges are "tight" and of a nearly loading and N independent size, for example, ~ 2 segments thick. In this Letter we construct a quantitative theory for ΔE based on a qualitatively different physical picture (sketched in Figure 1) that is consistent with strong adsorption and long-lived tight bridges, which we argue is valid for all loadings for the large ϵ_{pn} systems of interest. The key physics is the tight bridge NP coordination number and barrier for NP relative motion.

The idea that tight bridges dominate the dynamically long-lived polymer-mediated bonds between NPs seems natural given the strong confinement of bridging segments between adsorbing surfaces is akin to an ultrathin capped film.[30,31] It is also consistent with bridges being strong but short-ranged.[21,32] This perspective motivates our core hypothesis: the rate limiting elementary time scale and real space event for stress relaxation involves activated dilational motion of all NPs in a bridging complex on the segmental (~ 1 nm) scale in order to
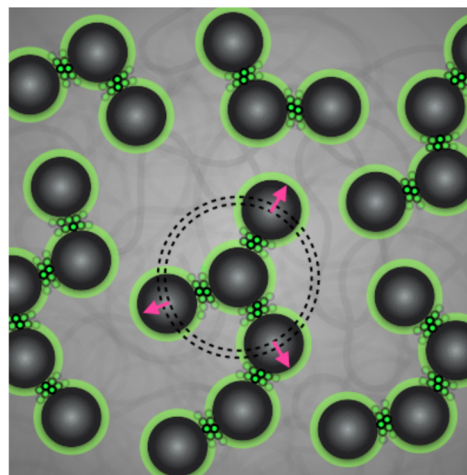
Figure 1. Schematic of the polymer−NP tight bridging complex structure. The small scale activated relative dilational motion of NPs is indicated by the pink arrows. Three classes of elementary polymer units are indicated: background matrix (gray), adsorbed interfacial layers (green shells), and bridging segments (green disks).

loosen confinement constraints on the bridging segments which triggers an irreversible rearrangement event that is the origin of the extra friction encoded in the rheological shift factor. Explicit treatment of polymer chain desorption is not relevant in our proposed physical scenario. Desorption of segments not in a tight bridging confined configuration can occur but, per dielectric experiments,[9,10] are viewed as much faster than bridging complex relaxation and thus enter via the first factor on the right-hand side of eq 1. In this sense, no single NP "glassy layers" are invoked. We refer to the key event as the "bridging complex local relaxation", and the appropriate theoretical object to quantify it is the NP potential-of-mean force (PMF). Our physical idea implies the dynamical physics in the shift factor is spatially local, consistent with it being the quantity that allows master curve construction for slower and longer length scale relaxation processes, and consistent with the relatively short-range of the PMF (a few segment diameters, per Figure 2c below) that controls NP dilational motion.

The physical idea sketched in Figure 1 implies ΔE is the product of the NP tight bridging coordination number (number of nanoparticle "bonds" per NP, not to be confused with the number of rubbery strands), n_B, and the corresponding PMF barrier, Δw, that must be surmounted via thermal fluctuation to achieve the relative displacement of all the bridging NPs associated with a local complex:

$$\Delta E \approx n_B \Delta w \tag{2}$$

Both n_B and Δw depend on equilibrium structure and are rich functions of ϕ, size ratio (D/σ), dimensionless total packing fraction (η), the bare interfacial attraction strength (ϵ_{pn}), and spatial range in units of segment size (α). The precise definition of a "tight bridge" is given below. Equation 2 is a qualitatively different conception of the "dynamically-relevant bridge" than the postulate[10] underlying $\Delta E \sim \epsilon_{pn} \langle h_{IPS} \rangle^{-2}$.

To implement eq 2 requires the NP pair correlation function, $g_{nn}(r)$. We compute it using the most accurate version of PRISM integral equation theory[33] with the modified-Verlet closure[34,35] (validated against simulation[25]) which predicts tight bridges for the strong short-range
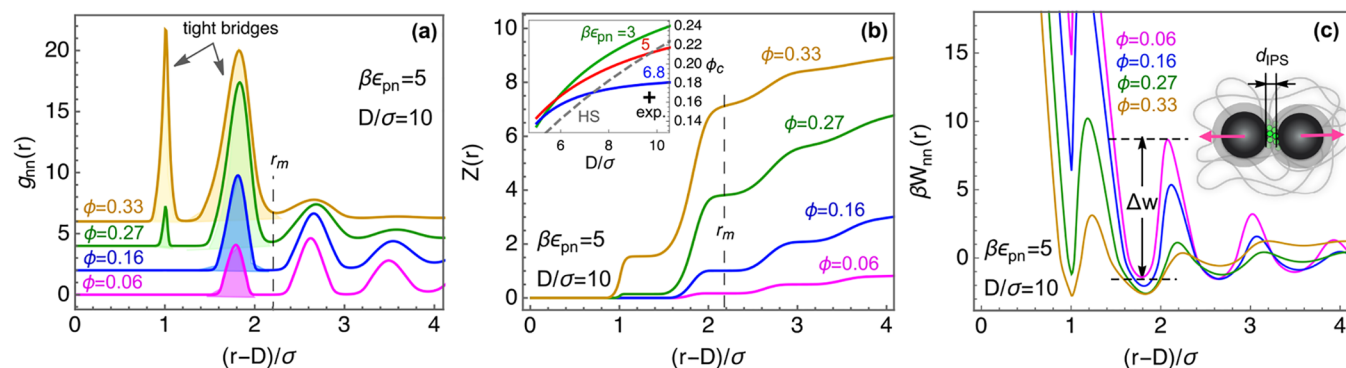
Figure 2. (a) NP pair correlation function, (b) cumulative NP coordination number, and (c) NP potential-of-mean force (PMF) as a function of reduced intersurface distance at different loadings for $\beta\epsilon_{pn} = 5$, $D/\sigma = 10$, and $\eta = 0.6$. For clarity, curves are shifted vertically in (a) by constants of 2, 4, 6 for $\phi = 0.16, 0.27, 0.33$, respectively. The dotted vertical line in (a) and (b) indicates the inter-NP separation where $Z(r_m) = n_B$. The inset of (b) shows the predicted size ratio dependence of the NP percolation threshold for several values of $\beta\epsilon_{pn}$ for the PNC (solid curves) and hard-sphere fluid (dashed curve) models; one silica−P2VP experimental data point[8] is shown (symbol). Panel (c) shows the NP PMFs and an example of how their barriers, Δw, are determined for $\phi = 0.06$. The cartoon depicts the reorganization event of a tight-bridge of two NPs (arrows are exaggerated).

attractions characteristic of miscible PNCs.[22,23,28] The corresponding PMF is $W_{nn}(r) = -k_B T \ln g_{nn}(r)$, from which one can determine Δw. A minimalist (validated against scattering measurements[29,36,37]) single effective interfacial energy model[23] is adopted: nanoparticles are hard spheres, polymers are semiflexible chains of tangentially connected hard-spheres or "beads"[38] of diameter σ and persistence length $l_p/\sigma = 4/3$, and the bead−NP attraction is $U_{pn}(r) = -\epsilon_{pn} e^{-(r-r_c)/\alpha\sigma}$ for $r > r_c$, where $r_c = (D + \sigma)/2$. The microscopic parameters are *a priori* chosen based on PRISM theory analysis of X-ray scattering patterns of silica−PV2P PNCs:[29] $\alpha = 0.5$, $\eta = (\rho_p\sigma^3 + \rho_n D^3)\pi/6 = 0.6$, $D/\sigma = 10$, $\phi = \rho_n D^3\pi/6 = 0-0.4$; values of $\beta\epsilon_{pn} = 3-7$ are explored to mimic different NP−polymer chemistries (all in the strong bridging regime). To connect with the experiments of present interest, we take $\sigma \sim 1.5$ nm (so $D \sim 15$ nm) and $N = 100$ corresponding to $2R_g/D \sim 1$; our results are insensitive to N beyond this value. Although PRISM theory predicts bridging-driven phase separation for the studied model,[23] all analysis here is in the globally homogeneous region.

Representative results for $g_{nn}(r)$ are shown in Figure 2a plotted as a function of intersurface distance $d_{IPS} \equiv r - D$ for $\beta\epsilon_{pn} = 5$. For $\phi < 0.27$, the first sharp and intense peak at $d_{IPS} \approx 2\sigma$ corresponds to the dominant and strongest tight bridging configuration. As NP loading increases, a tighter bridging peak emerges at $d_{IPS} \approx 1\sigma$. Importantly, the bridging configurations are very well-defined as indicated by the remarkably flat and nearly zero value of $g_{nn}(r)$ in the interstitial region; modest smearing occurs at higher loading due to many-particle effects (more NP neighbors). These pair correlations qualitatively differ from those of the hard-sphere (HS) fluid model[8] (see Figure S3).

Given the predicted migration inward of the first coordination shell with ϕ, we consider all NPs within $d_{IPS} \leq 2\sigma$ from a tagged NP as constituting "tight bridges". Figure 2b shows the cumulative NP coordination number as a function of distance r from the center of a tagged NP, $Z(r) = \int_0^r dr' 4\pi r'^2 \rho_n g_{nn}(r')$, at different ϕ values. The striking plateau of $Z(r)$ (absent for the HS model, see Figure S3) that emerges at $d_{IPS} \sim 2\sigma$ defines the NP tight bridge coordination number,

that is, $n_B = Z(r_m)$, where r_m is the first local minimum of $g_{nn}(r > D + 2\sigma)$.

Although the bond percolation threshold plays no special role in our theory for ΔE, we can employ the computed n_B to estimate it. Besides its relevance to viscoelasticity (a fit parameter in the sol−gel model[8]), it serves as another check on our structure calculations. We estimate the percolation threshold based on the criterion $n_B(\phi_c) = 2$. The inset of Figure 2b shows the size ratio dependence of ϕ_c for $\beta\epsilon_{pn} = 3, 5$, and 6.8. It increases with D/σ and tends to slowly saturate at large D/σ, trends in agreement with silica−P2VP experiments.[8] The experimental ϕ_c for $D/\sigma \sim 10$ is close to the $\beta\epsilon_{pn} = 6.8$ curve, an attraction energy quite similar to that independently deduced value of ~ 5.2 based on matching PRISM theory and X-ray scattering data for P2VP−silica PNCs.[29] The percolation threshold sensibly decreases with attraction strength. Analogous results for the HS fluid model are also shown and exhibit significant differences reflecting the absence of polymer-mediated bridging.

The ϕ-dependent PMF quantifies the free energy cost to bring two NPs from infinitely far apart to a fixed separation, r. A barrier is the difference between the PMF values at an adjacent local maximum and minimum, which are separated by a small distance of $\sim 0.5\sigma$. Figure 2c shows there are two tight bridging minima at $d_{IPS} \sim \sigma$ and $\sim 2\sigma$ denoted as s_1 and s_2, respectively. At low to moderate ϕ, only the s_2 state is relevant, and Δw is the difference between the local PMF minimum at $d_{IPS} \sim 1.8\sigma$ and the maximum at $d_{IPS} \sim 2.2\sigma$. The PMF barriers can be rather high ($\sim 6k_B T$) for tight bridging states ($d_{IPS} \sim 1-2\sigma$), which reflects generic local packing correlations in dense liquids. As loading increases, the local PMF minimum decreases modestly (stronger bridge), but the local maximum drops more rapidly, with the net result that the PMF barrier decreases with loading. The relative probability NPs are in the tightest s_1 state grows substantially at high loading, resulting in two PMF barriers becoming important. As discussed in SI, the two tight bridging states are accounted for in a simple, but no adjustable parameter, manner by computing an average PMF barrier determined via weighting the 2 contributions with the coordination number z_i in each shell for all ϕ, that is, $\Delta w = (z_1\Delta w_1 + z_2\Delta w_2)/(z_1 + z_2)$, which recovers the single s_2 barrier at low ϕ.
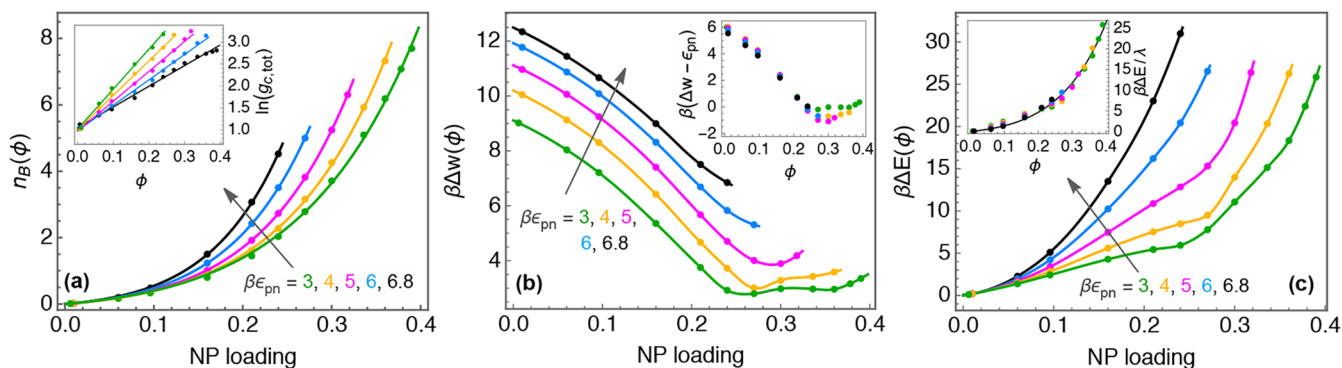
Figure 3. NP loading dependence of (a) tight bridge coordination number, (b) PMF barrier, and (c) activation energy $\Delta E = n_B \Delta w$, for $D/\sigma = 10$, $\eta = 0.6$, and varying attraction strength $\beta \epsilon_{np}$, as indicated. Solid curves in all main panels are guides to the eye except for (a), which are fits to $A \phi e^{B\phi}$. Insets: (a) log−linear plot of the contact value of $g_{nn}(r)$ vs ϕ with linear fits, (b) Δw vertically shifted by ϵ_{np}, and (c) collapse of $\beta \Delta E(\phi)$ scaled by λ with a master curve fit to $A' \phi e^{B'\phi}$ (see main text for details).

Figure 3 shows our main results: the NP tight bridging coordination number, PMF barrier, and dynamic activation barrier, as a function of loading and $\beta \epsilon_{np}$ for fixed $D/\sigma = 10$ and $\eta = 0.6$. For a given attraction strength, n_B grows strongly with NP loading, and the results are well described (Figure S6) by an exponential growth law, $n_B(\phi) = A \phi e^{B\phi}$, with $A \approx 2.2$ insensitive to $\beta \epsilon_{np}$ and $B = 0.86 \beta \epsilon_{pn} + 2.9$. This form is physically motivated by the predicted delta-function-like bridging peaks in $g_{nn}(r)$ at r_1 and r_2 (Figure 2). Since $n_B = \int_0^{r_m} 4\pi r'^2 \rho_n g_{nn}(r') $, it follows that roughly $n_B \sim \phi g_{c,tot}(\phi, \beta \epsilon_{pn})$, where $g_{c,tot} = g_{nn}(r_1) + g_{nn}(r_2)$. Numerically, we find $g_{c,tot}(\phi, \beta \epsilon_{pn}) = 2.71 e^{(1.13\beta\epsilon_{pn} + 1.26)\phi}$ (see inset of Figure 3a), leading to the above expression for n_B. Given $g_{nn}(r) = e^{-\beta W_{nn}(r)}$, this analysis also suggests a linear growth of the PMF minimum $-\beta W_{nn,min}$ with ϕ.

Figure 3b shows the PMF barrier (dominated by local minima of $g_{nn}(r)$) generally decreases with loading until tending to saturate at high ϕ. This decrease reflects the reduced free energy cost of a locally unfavorable separation of a tagged pair of NPs since there are more close by NPs at higher loading. Such behavior differs from the loading dependence of the bridging adsorption energy defined from the PMF minima (local maxima of $g_{nn}(r)$), which always deepens with growing ϕ. An interesting data collapse of the PMF barrier is predicted for different $\beta \epsilon_{pn}$ based on a vertical shift of Δw by ϵ_{pn} (inset of Figure 3b), suggesting a roughly additive dependence. Both n_B and Δw grow with $\beta \epsilon_{pn}$ and vary nonlinearly with loading which reflects correlated local structural changes beyond a naïve mean field picture.

Assembling these results in eq 2, the resultant ΔE is predicted to grow in a strongly upwardly curved nonlinear manner with both loading and attraction strength (Figure 3c). These dependences are much stronger than the growth of the thermodynamic interfacial cohesive energy density or cohesion per monomer (see Figure S8). The subtle curve wiggling at small $\beta \epsilon_{pn}$ reflects the weakly nonmonotonic behavior of the PMF barrier when $\phi > 0.25$ and our simple averaging model for the two tight bridging states. Strikingly, an excellent data collapse is achieved by rescaling ΔE with a $\beta \epsilon_{pn}$-dependent constant (inset of Figure 3c). This suggests that the dynamical consequences of ϕ and $\beta \epsilon_{pn}$ on the activation energy are (perhaps surprisingly) multiplicative. The numerical results are well fit by an exponential form: $\beta \Delta E(\phi, \beta \epsilon_{pn}) = A' \phi e^{B'\phi}$, with

$A' \approx 0.024(\beta \epsilon_{pn})^{3.6} + 6.88$ and $B' \approx 5.2$. A power law fit is inferior and less physically motivated (see SI).

The theoretical $\Delta E(\phi)$ results are compared to experiments (silica PNCs with PVAc,[10] PMMA,[16] and P2VP[9,39]) in Figure 4 by varying the single adjustable parameter $\beta \epsilon_{pn}$ that defines
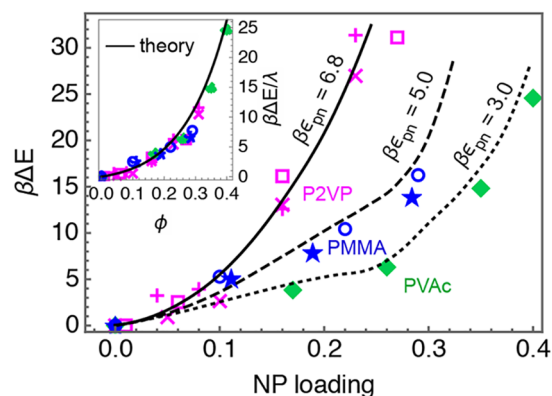
Figure 4. Experimental activation energies (symbols) for silica-based PNCs with different polymer chemistries (see text for refs.): PVAc (D = 14 nm, M_w = 40k (diamond)), PMMA (D = 15 nm, M_w = 49k (circle), 92k (star)), P2VP (D = 18 nm, M_w = 38k (square); D = 14 nm, M_w = 105k (plus), 554k (cross)). A reference temperature of 453 K is chosen for unit conversion. Theoretical predictions are smooth curves for $\beta \epsilon_{pn}$ = 3 (dotted), 5 (dashed), 6.8 (solid). Inset: collapse of rescaled experimental data $\beta \Delta E / \lambda$ compared to the theoretical master curve (same as inset of Figure 3c). Here, λ = 1, 2.1, and 5 for PVAc, PMMA, and P2VP, respectively.

the chemistry-specific segment-NP adsorption energy. The experimental data are extracted using $\ln\left(\frac{a_T(\phi)}{a_{T,0}}\right) = \frac{\Delta E(\phi)}{k_B}\left(\frac{1}{T} - \frac{1}{T_{ref}}\right)$ per eq 1, where T_{ref} is the reference temperature and $a_T(\phi)$ and $a_{T,0}$ are the PNC and pure polymer melt rheological shift factors, respectively. While the dielectric shift factors $a_{T,0}(\phi)$ were used[10] to characterize the polymer matrix dynamics at finite loadings, it is nearly invariant to NP loading[9,10] and agrees with the pure polymer melt rheological shift factor. Hence, different choices of $a_{T,0}$ have no significant effect on the resulting $\Delta E(\phi)$ (see SI). No obvious N-dependence of $\Delta E(\phi)$ is found for the PMMA and P2VP systems for which $2R_g$ or $R_{ee} \geq D$.

Figure 4 shows very good theory—experiment agreement for the silica—P2VP systems that are expected to have the largest interfacial attraction, with $\beta\epsilon_{pn}$ = 6.8 consistent with our percolation threshold analysis (inset of Figure 2b). For the PVAc and PMMA systems, the theoretical results using weaker attractions of $\beta\epsilon_{pn}$ = 3 and 5, respectively, are also in near quantitative accord with the ΔE data. The absolute and relative magnitudes of the attraction energies are chemically sensible and agree with the fact that PMMA—silica has a stronger attraction than PVAc—silica.[40] As a further test of the theoretically predicted multiplicative form of the ϕ and $\beta\epsilon_{pn}$ dependences of $\beta\Delta E$, we rescale the experimental ΔE data by a parameter λ = 1, 2.1, and 5 for the PVAc, PMMA, and P2VP systems, respectively. A good master curve is obtained as shown in the inset of Figure 4, and the functional form is in excellent agreement with the theory.

In summary, we have formulated the first microscopic theory for the elementary time scale of viscoelastic response in PNCs with strong interfacial cohesion. The key process is proposed to be a thermal fluctuation driven small relative dilational motion of NP pairs which facilitates reorganization of tight polymer bridges. The dynamic barrier or activation energy is a product of the NP tight bridge coordination number and associated PMF barrier. It grows nonlinearly with increasing interfacial attraction strength as a consequence of changes of confined interfacial polymer packing as embedded in the PMF. Notably, this rich dependence on interfacial cohesion does not, to leading order, modify the basic exponential growth of the activation energy with NP concentration. All the theoretical results are in good agreement with experiments.

We believe that the demonstrated level of theory—experiment agreement, along with verification of our predictions for master curve behavior, strongly supports our proposed idea that the dynamically relevant polymer—NP complexes involve tight bridging for all loadings. However, surprisingly, our theoretical calculations are also consistent with the phenomenological $\Delta E \sim \langle h_{IPS} \rangle^{-2}$ (and related) loading dependence discussed previously in this Letter (see Figure S2). But the underlying physical picture is different since it assumes a uniform NP distribution that conflicts with PRISM theory predictions and our theory for the dynamic shift factor. The present advance sets the stage for understanding other questions and systems such as the shift factor in polymer blends,[41,42] the role of NP size,[43] and PNC elastic modulus reinforcement at intermediate and low frequencies.

ASSOCIATED CONTENT

Supporting Information

The Supporting Information is available free of charge at https://pubs.acs.org/doi/10.1021/acsmacrolett.1c00732.

Experimental shift factor data for extracting activation barriers, additional methodological details, and supporting figures (PDF)

AUTHOR INFORMATION

Corresponding Author

Kenneth S. Schweizer − Departments of Materials Science, Chemistry, Chemical and Biomolecular Engineering, and Materials Research Laboratory, University of Illinois, Urbana, Illinois 61801, United States; Email: kschweiz@illinois.edu

Author

Yuxing Zhou − Departments of Materials Science and Materials Research Laboratory, University of Illinois, Urbana, Illinois 61801, United States; orcid.org/0000-0002-4476-0680

Complete contact information is available at:
https://pubs.acs.org/10.1021/acsmacrolett.1c00732

Notes

The authors declare no competing financial interest.

REFERENCES

(1) Kumar, S. K.; Benicewicz, B. C.; Vaia, R. A.; Winey, K. I. 50th Anniversary Perspective: Are Polymer Nanocomposites Practical for Applications? Macromolecules 2017, 50 (3), 714−731.

(2) Wu, H.; Fahy, W. P.; Kim, S.; Kim, H.; Zhao, N.; Pilato, L.; Kafi, A.; Bateman, S.; Koo, J. H. Recent Developments in Polymers/Polymer Nanocomposites for Additive Manufacturing. Prog. Mater. Sci. 2020, 111, 100638.

(3) Crosby, A. J.; Lee, J. Polymer Nanocomposites: The "Nano" Effect on Mechanical Properties. Polym. Rev. 2007, 47 (2), 217−229.

(4) Boccaccini, A. R.; Erol, M.; Stark, W. J.; Mohn, D.; Hong, Z.; Mano, J. F. Polymer/Bioactive Glass Nanocomposites for Biomedical Applications: A Review. Compos. Sci. Technol. 2010, 70 (13), 1764−1776.

(5) Bailey, E. J.; Winey, K. I. Dynamics of Polymer Segments, Polymer Chains, and Nanoparticles in Polymer Nanocomposite Melts: A Review. Prog. Polym. Sci. 2020, 105, 101242.

(6) Schneider, G. J. Dynamics of Nanocomposites. Curr. Opin. Chem. Eng. 2017, 16, 65−77.

(7) Song, Y.; Zheng, Q. Concepts and Conflicts in Nanoparticles Reinforcement to Polymers beyond Hydrodynamics. Prog. Mater. Sci. 2016, 84, 1−58.

(8) Chen, Q.; Gong, S.; Moll, J.; Zhao, D.; Kumar, S. K.; Colby, R. H. Mechanical Reinforcement of Polymer Nanocomposites from Percolation of a Nanoparticle Network. ACS Macro Lett. 2015, 4 (4), 398−402.

(9) Baeza, G. P.; Dessi, C.; Costanzo, S.; Zhao, D.; Gong, S.; Alegria, A.; Colby, R. H.; Rubinstein, M.; Vlassopoulos, D.; Kumar, S. K. Network Dynamics in Nanofilled Polymers. Nat. Commun. 2016, 7 (1), 11368.

(10) Yang, J.; Melton, M.; Sun, R.; Yang, W.; Cheng, S. Decoupling the Polymer Dynamics and the Nanoparticle Network Dynamics of Polymer Nanocomposites through Dielectric Spectroscopy and Rheology. Macromolecules 2020, 53 (1), 302−311.

(11) Cheng, S.; Carroll, B.; Bocharova, V.; Carrillo, J.-M.; Sumpter, B. G.; Sokolov, A. P. Focus: Structure and Dynamics of the Interfacial Layer in Polymer Nanocomposites with Attractive Interactions. J. Chem. Phys. 2017, 146 (20), 203201.

(12) Glomann, T.; Schneider, G. J.; Allgaier, J.; Radulescu, A.; Lohstroh, W.; Farago, B.; Richter, D. Microscopic Dynamics of Polyethylene Glycol Chains Interacting with Silica Nanoparticles. Phys. Rev. Lett. 2013, 110 (17), 178001.

(13) Jimenez, A. M.; Zhao, D.; Misquitta, K.; Jestin, J.; Kumar, S. K. Exchange Lifetimes of the Bound Polymer Layer on Silica Nanoparticles. ACS Macro Lett. 2019, 8 (2), 166−171.

(14) Bailey, E. J.; Griffin, P. J.; Composto, R. J.; Winey, K. I. Characterizing the Areal Density and Desorption Kinetics of Physically Adsorbed Polymer in Polymer Nanocomposite Melts. Macromolecules 2020, 53 (7), 2744−2753.

(15) Mujtaba, A.; Keller, M.; Ilisch, S.; Radusch, H.-J.; Beiner, M.; Thurn-Albrecht, T.; Saalwächter, K. Detection of Surface-Immobilized Components and Their Role in Viscoelastic Reinforcement of Rubber-Silica Nanocomposites. *ACS Macro Lett.* **2014**, *3* (5), 481−485.

(16) Cui, W.; You, W.; Yu, W. Mechanism of Mechanical Reinforcement for Weakly Attractive Nanocomposites in Glassy and Rubbery States. *Macromolecules* **2021**, *54* (2), 824−834.

(17) Polymer chemistries are denoted as follows: PMMA = poly(methyl methacrylate), PVAc = poly(vinyl acetate), P2VP = poly(2-vinylpyridine).

(18) De Gennes, P. G. Conformations of Polymers Attached to an Interface. *Macromolecules* **1980**, *13* (5), 1069−1075.

(19) Rubinstein, M.; Colby, R. H. *Polymer Physics*; Oxford University Press: USA, 2003.

(20) Long, D.; Lequeux, F. Heterogeneous Dynamics at the Glass Transition in van Der Waals Liquids, in the Bulk and in Thin Films. *Eur. Phys. J. E* **2001**, *4* (3), 371−387.

(21) Merabia, S.; Sotta, P.; Long, D. R. A Microscopic Model for the Reinforcement and the Nonlinear Behavior of Filled Elastomers and Thermoplastic Elastomers (Payne and Mullins Effects). *Macromolecules* **2008**, *41* (21), 8252−8266.

(22) Hall, L. M.; Schweizer, K. S. Structure, Scattering Patterns and Phase Behavior of Polymer Nanocomposites with Nonspherical Fillers. *Soft Matter* **2010**, *6* (5), 1015−1025.

(23) Hall, L. M.; Schweizer, K. S. Many Body Effects on the Phase Separation and Structure of Dense Polymer-Particle Melts. *J. Chem. Phys.* **2008**, *128* (23), 234901.

(24) Hooper, J. B.; Schweizer, K. S. Real Space Structure and Scattering Patterns of Model Polymer Nanocomposites. *Macromolecules* **2007**, *40* (19), 6998−7008.

(25) Zhou, Y.; Schweizer, K. S. PRISM Theory of Local Structure and Phase Behavior of Dense Polymer Nanocomposites: Improved Closure Approximation and Comparison with Simulation. *Macromolecules* **2020**, *53* (22), 9962−9972.

(26) Sorichetti, V.; Hugouvieux, V.; Kob, W. Structure and Dynamics of a Polymer-Nanoparticle Composite: Effect of Nanoparticle Size and Volume Fraction. *Macromolecules* **2018**, *51* (14), 5375−5391.

(27) Liu, J.; Gao, Y.; Cao, D.; Zhang, L.; Guo, Z. Nanoparticle Dispersion and Aggregation in Polymer Nanocomposites: Insights from Molecular Dynamics Simulation. *Langmuir* **2011**, *27* (12), 7926−7933.

(28) Molinari, N.; Sutton, A. P.; Mostofi, A. A. Mechanisms of Reinforcement in Polymer Nanocomposites. *Phys. Chem. Chem. Phys.* **2018**, *20* (35), 23085−23094.

(29) Zhou, Y.; Yavitt, B. M.; Zhou, Z.; Bocharova, V.; Salatto, D.; Endoh, M. K.; Ribbe, A. E.; Sokolov, A. P.; Koga, T.; Schweizer, K. S. Bridging-Controlled Network Microstructure and Long-Wavelength Fluctuations in Silica-Poly(2-Vinlypyridine) Nanocomposites: Experimental Results and Theoretical Analysis. *Macromolecules* **2020**, *53* (16), 6984−6994.

(30) Rittigstein, P.; Priestley, R. D.; Broadbelt, L. J.; Torkelson, J. M. Model Polymer Nanocomposites Provide an Understanding of Confinement Effects in Real Nanocomposites. *Nat. Mater.* **2007**, *6* (4), 278−282.

(31) Schweizer, K. S.; Simmons, D. S. Progress towards a Phenomenological Picture and Theoretical Understanding of Glassy Dynamics and Vitrification near Interfaces and under Nanoconfinement. *J. Chem. Phys.* **2019**, *151* (24), 240901.

(32) Payne, A. R. The Dynamic Properties of Carbon Black-Loaded Natural Rubber Vulcanizates. Part I. *J. Appl. Polym. Sci.* **1962**, *6* (19), 57−63.

(33) Schweizer, K. S.; Curro, J. G. Integral Equation Theories of the Structure, Thermodynamics, and Phase Transitions of Polymer Fluids. *Adv. Chem. Phys.* **2007**, *98*, 1−142.

(34) Verlet, L. Integral Equations for Classical Fluids: I. The Hard Sphere Case. *Mol. Phys.* **1980**, *41* (1), 183−190.

(35) Kinoshita, M. Interaction between Surfaces with Solvophobicity or Solvophilicity Immersed in Solvent: Effects Due to Addition of Solvophobic or Solvophilic Solute. *J. Chem. Phys.* **2003**, *118* (19), 8969−8981.

(36) Hall, L. M.; Anderson, B. J.; Zukoski, C. F.; Schweizer, K. S. Concentration Fluctuations, Local Order, and the Collective Structure of Polymer Nanocomposites. *Macromolecules* **2009**, *42* (21), 8435−8442.

(37) Kim, S. Y.; Schweizer, K. S.; Zukoski, C. F. Multiscale Structure, Interfacial Cohesion, Adsorbed Layers, and Thermodynamics in Dense Polymer-Nanoparticle Mixtures. *Phys. Rev. Lett.* **2011**, *107* (22), 225504.

(38) Honnell, K. G.; Curro, J. G.; Schweizer, K. S. Local Structure of Semiflexible Polymer Melts. *Macromolecules* **1990**, *23* (14), 3496−3505.

(39) Yavitt, B. M.; Salatto, D.; Zhou, Y.; Huang, Z.; Endoh, M.; Wiegart, L.; Bocharova, V.; Ribbe, A. E.; Sokolov, A. P.; Schweizer, K. S.; Koga, T. Collective Nanoparticle Dynamics Associated with Bridging Network Formation in Model Polymer Nanocomposites. *ACS Nano* **2021**, *15* (7), 11501−11513.

(40) Mortazavian, H.; Fennell, C. J.; Blum, F. D. Surface Bonding Is Stronger for Poly(Methyl Methacrylate) than for Poly(Vinyl Acetate). *Macromolecules* **2016**, *49* (11), 4211−4219.

(41) Genix, A.-C.; Bocharova, V.; Carroll, B.; Dieudonné-George, P.; Sztucki, M.; Schweins, R.; Sokolov, A. P.; Oberdisse, J. Direct Structural Evidence for Interfacial Gradients in Asymmetric Polymer Nanocomposite Blends. *ACS Appl. Mater. Interfaces* **2021**, *13* (30), 36262−36274.

(42) Ginzburg, V. V. Influence of Nanoparticles on Miscibility of Polymer Blends. A Simple Theory. *Macromolecules* **2005**, *38* (6), 2362−2367.

(43) Preliminary numerical theoretical study of the effect of NP size and surface area over the modest range $D/\sigma = 3−10$ finds ΔE is nearly invariant to changing NP size at fixed loading, PNC total packing fraction, and bare interfacial attraction strength.